A Background Investigation of Tornado Activity across the Southern Cumberland Plateau Terrain System of Northeastern Alabama

ANTHONY W. LYZA AND KEVIN R. KNUPP

Department of Atmospheric Science, Severe Weather Institute–Radar and Lightning Laboratories, University of Alabama in Huntsville, Huntsville, Alabama

(Manuscript received 23 August 2018, in final form 5 October 2018)

ABSTRACT

The effects of terrain on tornadoes are poorly understood. Efforts to understand terrain effects on tornadoes have been limited in scope, typically examining a small number of cases with limited observations or idealized numerical simulations. This study evaluates an apparent tornado activity maximum across the Sand Mountain and Lookout Mountain plateaus of northeastern Alabama. These plateaus, separated by the narrow Wills Valley, span ~5000 km^2 and were impacted by 79 tornadoes from 1992 to 2016. This area represents a relative regional statistical maximum in tornadogenesis, with a particular tendency for tornadogenesis on the northwestern side of Sand Mountain. This exploratory paper investigates storm behavior and possible physical explanations for this density of tornadogenesis events and tornadoes. Long-term surface observation datasets indicate that surface winds tend to be stronger and more backed atop Sand Mountain than over the adjacent Tennessee Valley, potentially indicative of changes in the low-level wind profile supportive to storm rotation. The surface data additionally indicate potentially lower lifting condensation levels over the plateaus versus the adjacent valleys, an attribute previously shown to be favorable for tornadogenesis. Rapid Update Cycle and Rapid Refresh model output indicate that Froude numbers for the plateaus in tornadic environments are likely supportive of enhanced low-level flow over the plateaus, which further indicates the potential for favorable wind profile changes for tornado production. Examples of tornadic storms rapidly acquiring increased low-level rotation while reaching the plateaus of northeast Alabama are presented. The use of this background to inform the VORTEX-SE 2017 field campaign is discussed.

1. Introduction

The role of underlying topography on tornado behavior has long been a subject of folklore in the United States (e.g., Doswell 2014; McDonald 2014), but the effects of topography on the evolution of severe thunderstorms and tornadoes are not well understood. Though the subject of many myths across tornado-prone regions of the United States, little comprehensive study has been executed on specifically how substantial topographic features may impact severe convection and tornadoes, including the mesoscale environment. Most observational studies investigating the impact of topography on severe storm or tornado behavior have focused on singular events, such as studies of the role of flow channeling up the Hudson River valley in modifying the near-storm environment of tornadic storms on 29 May 1995 (Bosart et al. 2006) and 31 May 1998 (LaPenta et al. 2005), but the conclusions of these studies are based on limited observations. Additional observational case studies have been performed on the role of topography on tornadic storms in the mountains around Huntsville, Alabama (Goodman and Knupp 1993; Knupp et al. 2014); the Sacramento Valley of Northern California (Braun and Monteverdi 1991); the Grand Teton Mountains and Yellowstone National Park in western Wyoming (Fujita 1989); the Appalachian Mountains of central Pennsylvania (Forbes 1998); the Rocky Mountains of northern and central Colorado (Nuss 1986; Bluestein 2000); the Rocky Mountain foothills of northern Colorado and southern Wyoming (Geerts et al. 2009); rolling hills across central Alabama (Karstens et al. 2013); the Cumberland Plateau and Great Tennessee Valley of east Tennessee (Gaffin and Parker 2006; Schneider 2009; Shamburger 2012); and the Sequoia National Park in California (Monteverdi et al. 2014). More recent work has focused on using mobile Doppler radar and data from WSR-88D radar sites in a geographical information

Corresponding author: Anthony W. Lyza, lyzaa@nsstc.uah.edu

DOI: 10.1175/MWR-D-18-0300.1

system (GIS) framework in order to seek correlations between topography and land surface roughness and tornado intensity (Houser et al. 2017). Results from the Houser et al. study showed statistically significant relationships between land elevation and tornado intensity for a limited number of tornadoes sampled by mobile radars over small terrain variations (a few tens of meters), but those relationships were split evenly between events where higher elevations were correlated to higher intensity and events where lower elevations were correlated to higher intensity.

Likewise, numerical simulation studies of the role of topography on tornadic or potentially tornadic storms are also limited. Markowski and Dotzek (2011) performed idealized numerical simulations of supercells moving over significant topographic features and their near-storm environments using the Bryan Cloud Model 1 (CM1; Bryan and Fritsch 2002). A tendency for increased convective inhibition (CIN) at lower elevations and modifications of shear due to flow changes in the near-storm environment around the topographic features were noted in the CM1 simulations. Lewellen (2012) undertook large-eddy simulation (LES) of idealized tornado-scale vortices over various terrain features and found variations in vortex behavior based on the type and orientation of terrain. A somewhat common feature in the simulations was the event of a corner flow collapse (Lewellen and Lewellen 2007), where a collapse in the corner region of the tornado vortex leads to a rapid increase in the convergence of angular momentum at the surface, leading to a rapid intensification of the tornado vortex near the surface. The occurrence of corner flow collapse, however, has never been observed in nature (Bluestein et al. 2014), which, compounded by the numerous outcomes of the LES, leads to considerable variability and uncertainty in determining how topography may directly impact tornado structure.

The problem of how topography may influence the evolution of tornadic storms is of particular interest in the southeastern United States, where the climatological maximum in major tornado activity (Coleman and Dixon 2014) intersects significant topography (and surface roughness) located at the southern end of the Appalachian Mountain system. The Sand Mountain and Lookout Mountain plateaus in northeastern Alabama form the southern end of the larger Cumberland Plateau system that extends into east Tennessee and eastern Kentucky. Together, Sand Mountain, Lookout Mountain, and the narrow, shallow Wills Valley that separates the two plateaus form the Southern Cumberland System (SCS; Fig. 1) that covers a geographical area of $\sim$5000 km^2. Besides lying within a broader swath of enhanced tornado activity climatologically, the SCS lies within an apparent climatological maximum in tornado activity that extends to its southwest into western and central Alabama and to its northeast into southern east Tennessee (Fig. 2).

This initial, preliminary paper details the statistics of tornadoes within the SCS region and highlights examples of rapid convective evolution and intensification of storm-scale rotation as parent storms reach the region. Surface observations, both from atop the SCS and within the neighboring Tennessee Valley, and Rapid Refresh (RAP) and Rapid Update Cycle (RUC) model soundings upstream of the SCS are analyzed in order to gain first-order insights into how the low-level flow and thermodynamics may change across the topography. Hypotheses are developed for potential physical causes for enhanced tornado activity in the SCS, including potential modification of the low-level flow and the near-storm thermodynamic environment through topographic influence. These initial analyses are developed in order to form the background for intensive analysis of severe storm environments across the SCS. It serves as a building block for how subsequent studies utilizing myriad surface and remote sensing observations, as well as numerical simulations, have been developed. Plans for hypothesis testing of data gathered from the Verification of the Origins of Rotation in Tornadoes Experiment Southeast (VORTEX-SE) field campaign are discussed.

2. Background

The SCS resides at the northeastern edge of one of the most tornado-prone regions in the United States. This corridor, colloquially referred to as ''Dixie Alley'' (Dixon et al. 2011), spans from central Mississippi to northern Alabama and is the most vulnerable region in the United States to tornadoes due to several risk factors. These risk factors are multifold and rooted in both meteorological and sociological causes. The longevity, size, and intensity of tornadoes in Dixie Alley are among the most severe of any region in the United States, with a particular disparity in pathlength (and, thus, area exposed to tornado winds) in Dixie Alley versus the Great Plains or the Midwest (Coleman and Dixon 2014). Societal factors, such as population density, mobile home stock, the lack of a well-defined tornado season, and the nocturnal timing of many southeastern U.S. tornado events, compounds the vulnerability of the population to these large, destructive tornadoes, as well as a high occurrence of tornado activity overall (Ashley 2007; Ashley et al. 2008; Kis and Straka 2010; Krocak and Brooks 2018). Furthermore, an analysis of tornadogenesis patterns for the tornadoes that have impacted the SCS reveals that a distinct concentration

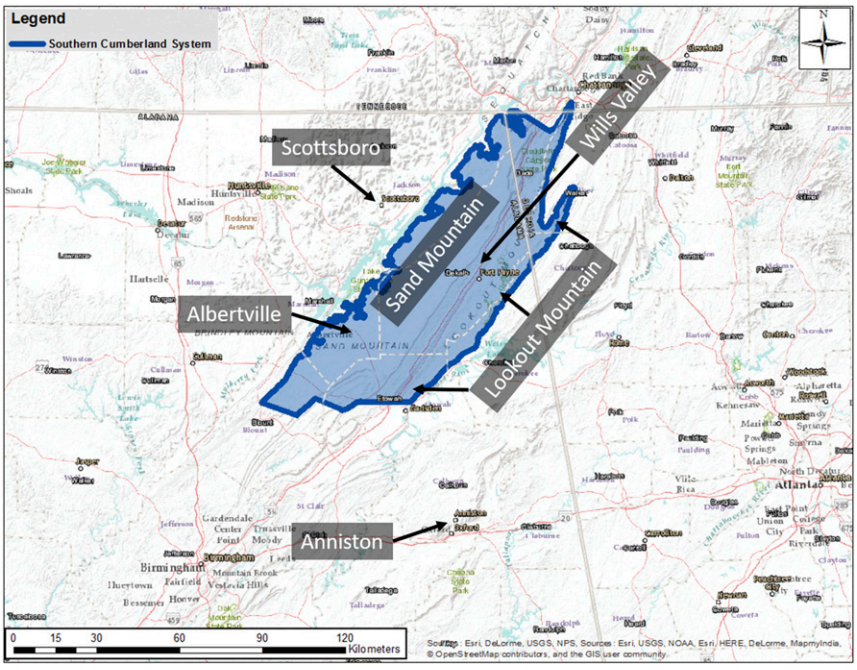

FIG. 1. A map highlighting the location of the SCS across northeastern Alabama, far northwestern Georgia, and a sliver of southern east Tennessee. The Sand Mountain and Lookout Mountain plateaus are labeled, with the Wills Valley dividing them and the Tennessee Valley situated just northwest of Sand Mountain just outside the northwestern edge of the SCS. The locations of the Scottsboro and Albertville surface observing sites and the RAP/RUC sounding site at Anniston are also denoted.

of tornadogenesis events has occurred along the northwestern edge of the SCS, known as the Sand Mountain plateau (the largest constituent of the SCS by land area; Fig. 3). Of the 79 tornadoes that affected the SCS from 1992 to 2016, 51 formed atop the Sand Mountain plateau. Of those 51 tornadoes, 24 (47%) have formed within 5 km of the northwestern edge, which represents roughly 20% of the plateau surface area (typical width of approximately 25 km). By comparison, only 10 total tornadogenesis events of any parent storm mode have been recorded in the Tennessee Valley, a valley that spans approximately 5–10 km in width between the northwestern edge of Sand Mountain and the rough hills and small mountains of northern Marshall and northwestern Jackson Counties, during the same time period from 1992 to 2016.

To determine whether or not this apparent clustering of tornadogenesis points along the northwestern side of Sand Mountain is statistically significant, an optimized hot spot analysis of tornadogenesis clustering was performed using the ArcGIS software package (ArcGIS 2018). The optimized hot spot analysis utilizes the Getis–Ord local statistic (G_i^*; Getis and Ord 1992) to identify areas of clustered occurrence of an event within a domain. Because G_i^* is a z score, a corresponding p value and confidence level can be computed to test for statistical significance of a potential cluster of events. The optimized hot spot analysis was performed for a domain defined as a region within 250 km of the SCS. This domain, although somewhat subjective in its selection, was employed in order to allow for a meaningful result to be gained through the analysis by balancing the resolution at which the analysis was performed while maintaining a sample size necessary for statistically significant results. In performing the hot spot analysis for equally sized polygon cells, the optimized hot spot analysis increases the cell size with increasing domain size. Therefore, defining a larger domain would decrease resolution in the analysis and promote aliasing of smaller-scale hot and cold spots, whereas using a smaller domain would lead to sample size issues and a lack of ability to generate statistically significant results. After the G_i^* scores and p values are calculated, a false discovery rate correction (e.g., Ventura et al. 2004) is performed in order to reduce the chances of falsely identifying cells as being statistically significant hot or cold spots.

The optimized hot spot analysis domain yielded an analysis performed at a cell size of 123.09 km^2, or a length of 11.09 km per side of each square cell. A large

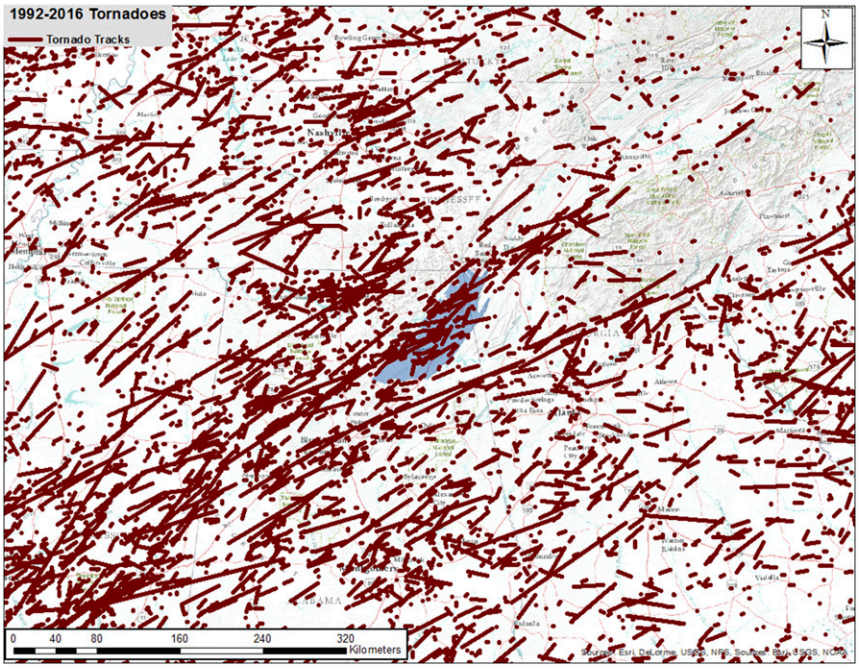

FIG. 2. Overview map of official tornado tracks across a portion of the southeastern United States from 1992 to 2016, with the SCS highlighted in blue.

swath of cells from west-central Alabama, near Tuscaloosa, to north-central and northeast Alabama and southern middle Tennessee were identified as hot spots at a 99% confidence interval for the domain consisting of the area within 250 km of the SCS (Fig. 4a). At first glance, this result may seem to suggest that the SCS is simply part of a larger region representing a climatological maximum of tornadogenesis, when compared to the entire analysis area. However, a closer inspection of the p values associated with each cell indicates that two relative p value minima (and corresponding confidence level/statistical significance maxima) exist within this broad cluster of hot spot cells. The absolute maximum, with p value minima of $O(10^{-12})$ or less, exists from the west edge of Huntsville, Alabama, westward to near Florence, Alabama. Given that the p values are inversely proportional to the confidence level at which the null hypothesis (that a given cell does not represent a hot spot in tornadogenesis) can be rejected, the p value minima represent cells where there is a maximum in confidence that a tornadogenesis hot spot is represented. Though this area may be produced by both physical and sociological causes, it will not be discussed further in this study.

The second relative maximum in tornadogenesis is identified over the northwestern portion of the SCS, with a p value minimum magnitude of $O(10^{-10})$. The minimum pixels are located within one of the least densely populated portions of the SCS, northeast of Albertville, Alabama. Furthermore, the extension of hot spot cells with at least 90% confidence all the way up the SCS to Chattanooga, Tennessee, is particularly notable given the lack of tornadogenesis points evident in immediately adjacent areas to the north of the SCS, some of which were included in the analysis of those cells. Therefore, the spine of statistical hot spot cells along the SCS is produced by the local tornadogenesis pattern atop the SCS, particularly along Sand Mountain. The extension of the tornadogenesis maximum past the SCS into southern east Tennessee, around Chattanooga, might be a product of the high population density of the Chattanooga metropolitan area, much higher than the population density of the SCS or any of the surrounding areas between Chattanooga and Huntsville. The goal of this study, therefore, is to highlight potential physical causes for why this statistical hot spot in tornadogenesis exists over the SCS and what role the terrain of northeastern Alabama plays in its existence.

3. Data and methodology

Historical data on SCS tornadoes were taken from the official Storm Data publication, managed by the National Centers for Environmental Information (NCEI 2018). Parent storm mode was divided into a simple

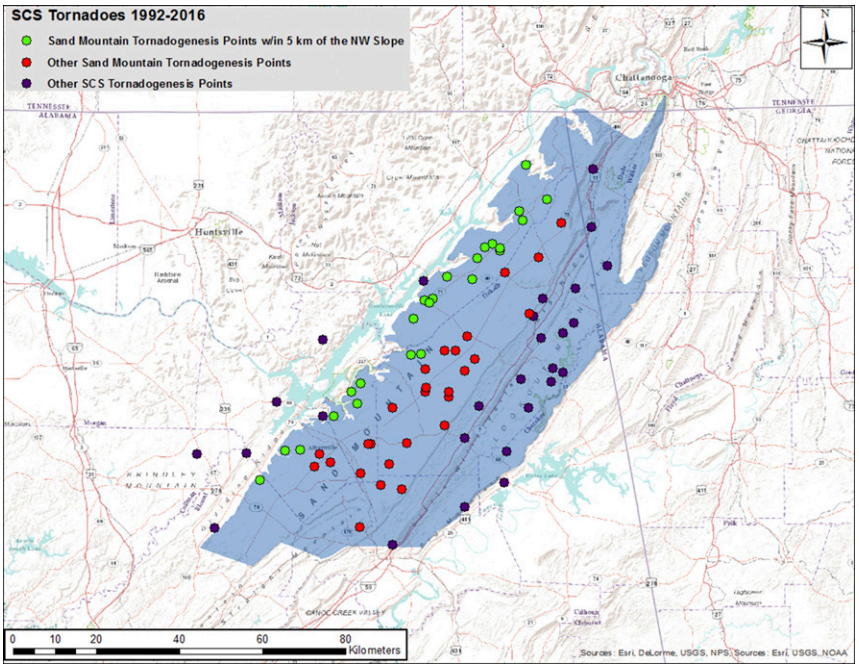

FIG. 3. Tornadogenesis locations for all tornadoes that impacted the SCS from 1992 to 2016. All dots (red, green, and purple) collectively represent all SCS tornadoes, red and green dots represent tornadoes that formed atop Sand Mountain, and green dots represent tornadoes that formed atop Sand Mountain within 5 km of the northwestern slope.

two-mode classification scheme of supercell and quasi-linear convective system (QLCS). Storm mode was determined for all SCS tornadoes dating back to 1992 using a combination of the Weather Surveillance Radar–88 Doppler (WSR-88D) sites at Hytop, Alabama (KHTX); Birmingham, Alabama (KBMX); and Peachtree City, Georgia (KFFC); the WSR-74C Doppler radar at Huntsville, Alabama (KHSV), over the 1992–2005 period; and the Advanced Radar for Operational and Meteorological Research (ARMOR;[1] Petersen et al. 2005), a radar jointly operated by the University of Alabama in Huntsville (UAH) and WHNT-TV in Huntsville. The resulting dataset consists of 79 tornadoes—46 from supercells and 33 from QLCSs—with the observed tornadoes spanning the EF0–EF5 range of the enhanced Fujita (EF) scale (Marshall et al. 2004; Table 1). A summary analysis of statistics regarding SCS tornadoes is provided in section 4.

Utilizing scanning Doppler radar in complex terrain presents significant challenges. One analysis that can be done with minimal consequence from changes in underlying topography is the single-Doppler analysis of the rotational velocity (V_{ROT}) of a circulation, estimated by fitting radial velocities to the radial profile of a Rankine combined vortex (Rankine 1901). The Rankine vortex profile is defined by the horizontal profile of tangential velocity as

$$V = \begin{cases} V_{max}\dfrac{R}{R_{max}}, & R \le R_{max} \\ V_{max}\dfrac{R_{max}}{R}, & R > R_{max} \end{cases}, \quad (1)$$

where V is the tangential wind speed, R is the radius from the circulation center, V_{max} is the maximum tangential velocity of the circulation, and R_{max} is the radius where V_{max} is located. By applying this assumption to radar data, values of V_{ROT} can be estimated from

$$V_{ROT} = \frac{V_{out} - V_{in}}{2}\cos\theta, \quad (2)$$

where V_{out} is the maximum outbound radial velocity, V_{in} is the minimum outbound (maximum inbound) radial velocity, and θ is the radial angle between V_{out} and V_{in} (e.g., $\cos\theta = 0$ if the radius of V_{out} and V_{in} from the scanning radar is the same; Desrochers and Harris 1996). Incorporating the $\cos\theta$ term eliminates divergent flow from the V_{ROT} calculation. This procedure has obvious drawbacks. Radial and vertical flows are neglected in

[1] The ARMOR was an upgrade (dual polarization initially, followed by larger antenna dish and radome) to the previous WSR-74C radar and was operational in 2005.

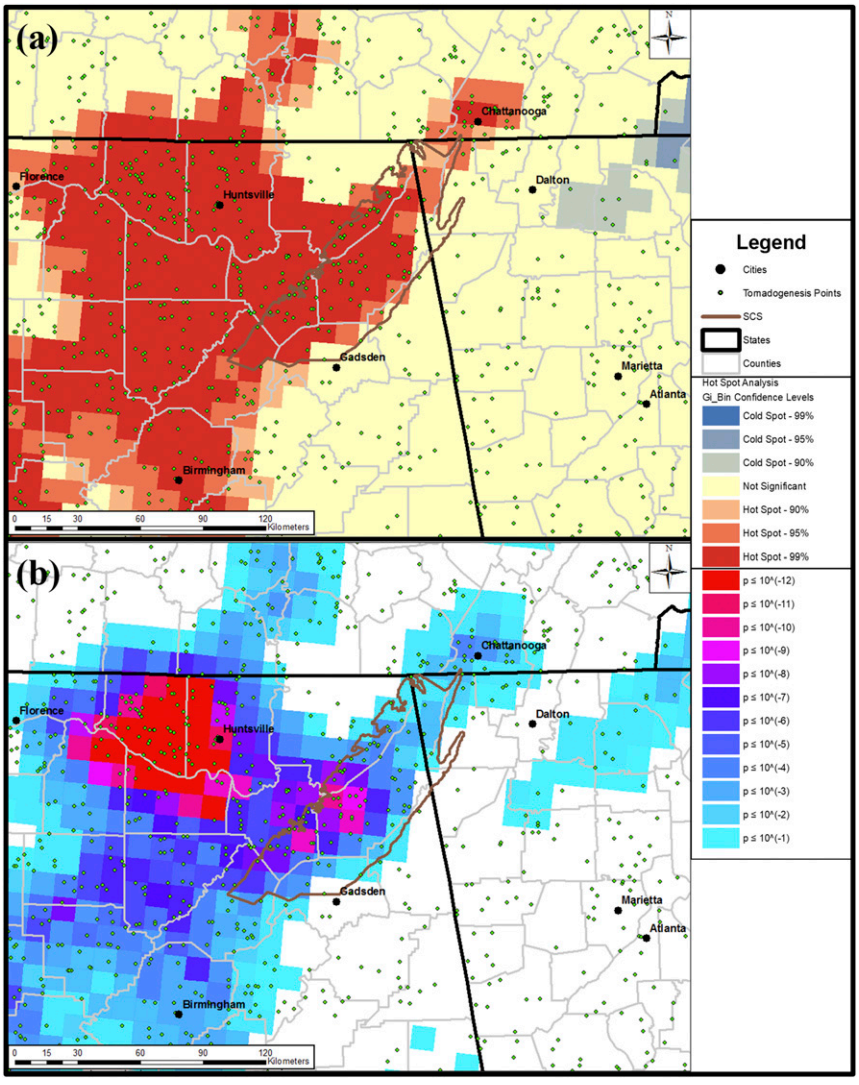

FIG. 4. (a) Optimized hot spot analysis results for hot and cold spots of tornadogenesis within 250 km of the SCS from 1992 to 2016, expressed in 90%, 95%, and 99% confidence levels of rejecting a null hypothesis that each cell is not a hot or cold spot for tornadogenesis in the domain. (b) The p values associated with each pixel from the optimized hot spot analysis.

the Rankine vortex profile, both of which have been shown to be very significant in supercell mesocyclone and QLCS mesovortex flows. These stark limitations force such analyses to produce more qualitative than quantitative results, with the most robust statements limited to general inferences about circulation intensity. In addition, this technique is difficult to perform in the cases of QLCS tornadoes, where mesovortices may not even be present prior to the parent QLCS reaching Sand Mountain. This analysis is performed for an EF4 tornado on 27 April 2011, illustrated in section 7a.

In the majority of cases, data aside from WSR-88D radar data are limited to automated weather observing station (AWOS) data from sites at Albertville (K8A0; atop Sand Mountain at 315 m ASL) and Scottsboro (K4A6; in the Tennessee Valley at 198 m ASL). The AWOS surface data were examined within 6 h prior to first tornadogenesis for events going back to 18 March 2013, the first event for which K4A6 was operating. Surface wind speed, direction, and terrain-parallel and terrain-perpendicular wind components were analyzed. The components of flow were calculated in order to attempt to gain meaningful insight into potential physical processes, including the blocking of flow by terrain, acceleration of flow over terrain, and channeling of flow within the Tennessee Valley. The surface observations were stratified by boundary layer type (approximated by

TABLE 1. Summary table of all SCS tornado events from 1992 to 2016.

Date (UTC)	EF0	EF1	EF2	EF3	EF4	EF5	Total	Injuries[a]	Fatalities	Supercell	QLCS
22 Nov 1992	1	1	3	0	0	0	5	31	0	0	5
27 Mar 1994	0	0	1	1	0	0	2	50	0	2	0
16 Feb 1995	0	0	1	1	0	0	2	133	6	2	0
16 Mar 1996	0	1	0	0	0	0	1	2	0	1	0
6 Jan 1997	1	0	0	0	0	0	1	0	0	0	1
22 Apr 1997	0	0	1	0	0	0	1	10	0	1	0
9 Apr 1998	0	1	0	0	0	0	1	0	0	1	0
17 Apr 1998	0	1	0	0	0	0	1	0	0	1	0
27 Apr 1999	2	0	0	0	0	0	2	0	0	2	0
24 Nov 2001	0	1	2	0	0	0	3	4	2	3	0
30 Mar 2002	0	1	0	0	0	0	1	0	0	1	0
19 Mar 2003	1	3	0	0	0	0	4	3	0	4	0
6 May 2003	0	1	0	0	0	0	1	0	0	0	1
22–23 Apr 2005	2	0	0	0	0	0	2	0	0	2	0
8 Apr 2006	1	0	0	0	0	0	1	0	0	1	0
22 Sep 2006	0	1	0	0	0	0	1	0	0	1	0
4 Apr 2007	0	1	0	0	0	0	1	0	0	0	1
6 Feb 2008	0	0	0	0	1	0	1	12	1	1	0
20 May 2008	1	0	0	0	0	0	1	0	0	1	0
29 Mar 2009	1	1	0	0	0	0	2	0	0	0	2
10 Apr 2009	1	0	0	1	0	0	2	5	0	1	1
20 Apr 2009	1	2	0	0	0	0	3	14	1	0	3
28 Jun 2009	1	0	0	0	0	0	1	0	0	1	0
25 Apr 2010	0	0	0	2	1	0	3	50	0	3	0
25 Oct 2010	1	1	1	0	0	0	3	0	0	0	3
26 Oct 2010	1	1	0	0	0	0	2	0	0	2	0
27–28 Apr 2011	0	7	3	0	1	1	12	50	40	3	9
18 Mar 2013	0	1	2	0	0	0	3	10	0	0	3
21 Feb 2014	0	0	1	0	0	0	1	1	0	0	1
29 Apr 2014	1	4	2	1	0	0	8	0	0	8	0
3 Oct 2014	1	0	0	0	0	0	1	0	0	0	1
4 Apr 2015	1	2	0	0	0	0	3	0	0	2	1
19 Apr 2015	1	0	0	0	0	0	1	0	0	0	1
30 Nov 2016	0	1	0	1	0	0	2	9	4	2	0
Total	19	32	17	7	3	1	79	384	54	46	33

[a] The injury totals given in this chart are certainly an underestimate of actual injury totals for tornadoes atop the SCS. For example, the EF5 tornado that impacted several communities on Sand Mountain on 27 April 2011 was responsible for 25 fatalities but officially has 0 injuries listed in Storm Data.

time of day): daytime[2] boundary layer (DBL; 1700–2259 UTC), afternoon–evening transition (AET; 2300–0459 UTC), mature nocturnal boundary layer (NBL; 0500–1059 UTC), and early convective boundary layer (EBL; 1100–1659 UTC). Additionally, because relative humidity has a substantial long-term high bias at K8A0, compared to surrounding stations, the first cloud layer [the lowest height at which the sky condition can be characterized as "broken"; MoDOT (2018)] derived from ceilometers was compared for the same time periods as proxies for LCL height. These results are discussed in section 5.

Finally, to better understand the environments of SCS tornadoes and to further inform hypotheses as to how the topography of the SCS may impact the near-storm environment, analyses of RUC and RAP model soundings were performed for events dating back to 2006. To evaluate the possibility of flow acceleration over the plateaus, Anniston, Alabama, was used as a consistent site to diagnose the wind and thermodynamic profiles upstream of the SCS. Anniston was chosen as the location of upstream sounding analysis in order to minimize any impacts from surrounding terrain and to compromise between analysis of the environment upwind to the SCS relative to the mean boundary layer flow and relative to the terrain-perpendicular component of flow. Data from the UAH-Severe Weather Institute–Radar and Lightning Laboratories (SWIRLL) Mobile Meteorological Measurement Vehicle (M3V)—a mobile mesonet

[2] The term "daytime boundary layer" was used instead of "convective boundary layer" to indicate that many of the diurnal boundary layer cases did not feature the dry neutral or unstable static stability conditions typically associated with a classical CBL.

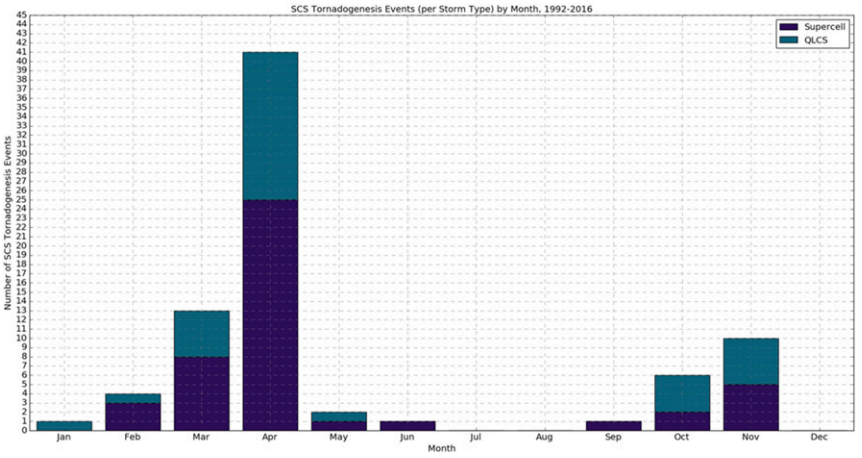

FIG. 5. SCS tornado distribution by month from 1992 to 2016, stratified by parent storm mode.

with temperature, relative humidity, pressure, wind, and solar radiation instrumentation approximately 3 m AGL—is used to illustrate the possibility of downslope wind formation that the RUC and RAP soundings suggest may occur. Additional details on the use of RUC and RAP soundings and the M3V in the analysis of SCS environments are given in section 6.

4. Climatological analysis of SCS tornadoes

The authors analyzed attributes of all SCS tornado events dating back to 1992, yielding a 25-yr dataset through 2016 (Table 1). A total of 79 tornadoes were officially recorded during the time frame across 34 different events. In total, these tornadoes were responsible for 54 fatalities and over 384 injuries. Supercells made up a majority of the parent storm mode for SCS tornadoes, with 46 supercell tornadoes versus 33 QLCS tornadoes. Fifty-one of the tornadoes that impacted the SCS from 1992 to 2016 formed atop the Sand Mountain plateau, 11 formed on the Lookout Mountain plateau, nine formed in the Wills Valley, and only eight formed outside the SCS and moved into the region. All damage intensities have been documented across the SCS since 1992, with 51 weak tornadoes (19 F/EF0 and 32 F/EF1), 24 strong (17 F/EF2 and seven F/EF3), and four violent tornadoes (three EF4 and one EF5). SCS tornadoes are most frequent during April, with 41 tornadoes across 14 cases, followed by March (13 tornadoes across six cases), November (10 tornadoes across three cases), and October (six tornadoes across three cases). This distribution of tornadoes leads to two evident peaks in SCS activity, with the primary peak during the early to middle of spring and the secondary peak across middle to late autumn (Fig. 5). An hourly distribution of tornado activity across the SCS shows that there is very little overall preference for any given time of day for collective tornado activity (Fig. 6). However, breaking down tornadoes by parent storm mode indicates a clear bimodality in favored time of day for supercell and QLCS tornadoes, with supercell tornadoes favored from midafternoon through about midnight local standard time (LST; UTC − 6) and QLCS tornadoes favored from around midnight to midmorning. Thus, the QLCS tornadoes have been favored during the nocturnal to early morning periods when the boundary layer exhibits greater static stability.

5. Surface observations ahead of SCS tornadoes

The AWOS surface data (see section 3) were examined within the 6-h period prior to tornadogenesis of SCS tornado events dating back to 2013. These data were then stratified into the four time periods to approximate different boundary layer time periods defined in section 3. Albertville (atop Sand Mountain) was noted to have a general tendency toward higher surface wind speeds than Scottsboro (in the Tennessee Valley), with a mean of 4.9 m s^{-1} (standard deviation of 1.7 m s^{-1}) at Albertville and 4.2 m s^{-1} (standard deviation of 2.0 m s^{-1}) at Scottsboro. Furthermore, a consistent pattern appears in wind direction as well, with more veered wind directions observed at Scottsboro (mean of 193°; standard deviation of 52°) than at Albertville (mean of 173°; standard deviation of 29°; Fig. 7). A clear pattern of greater positive terrain-perpendicular wind atop Sand Mountain than in the Tennessee Valley is evident in these cases. Although a collection of all observations shows no such discernable pattern in terrain-parallel wind, a general pattern can be seen when stratified by time period. During the AET and NBL (stable BL) time periods, terrain-parallel wind tends to be greater in the Tennessee Valley than atop Sand

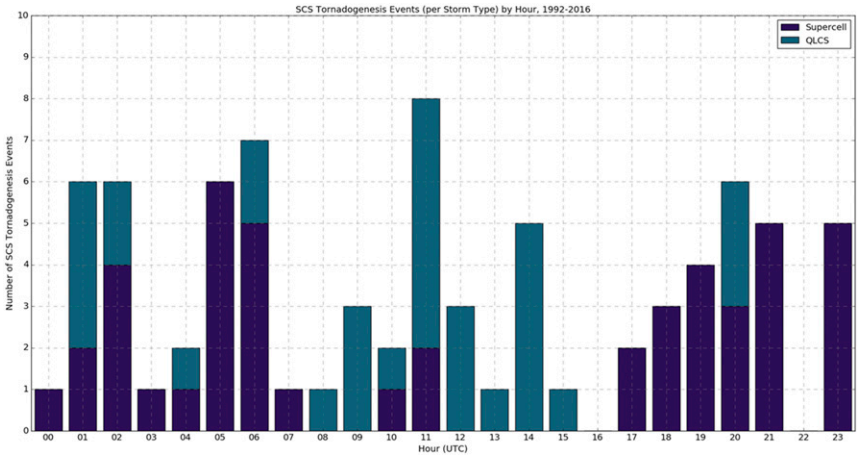

FIG. 6. SCS tornado distribution by UTC hour from 1992 to 2016, stratified by parent storm mode.

Mountain, though the reverse tends to be true during the DBL, when the terrain-parallel wind tends to be higher atop Sand Mountain than in the Tennessee Valley.

A similar comparative analysis was performed for first cloud layers from the ceilometers at K8A0 and K4A6. These data are used as proxies for LCL height, which has been found to be a meaningful discriminator in significant tornado versus nontornadic environments, with low LCL (and thus cloud base) heights being more conducive to tornadogenesis (Rasmussen and Blanchard 1998;

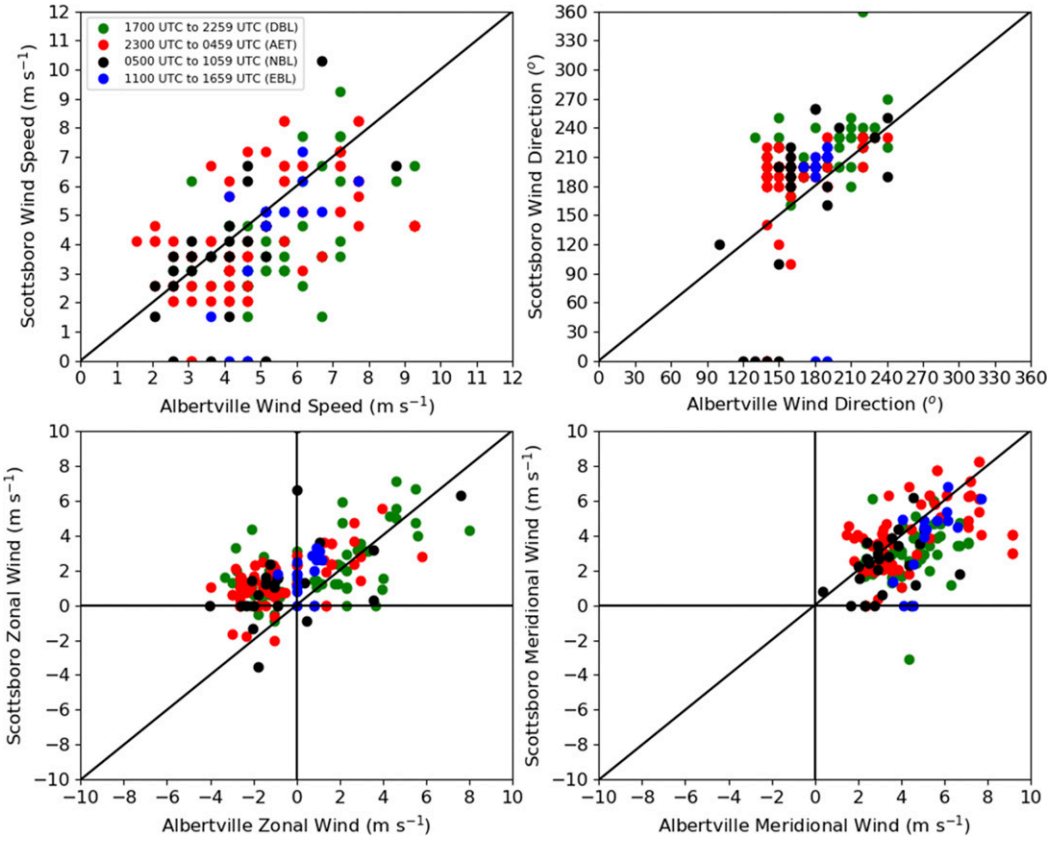

FIG. 7. Scatterplots of (top left) wind speed, (top right) wind direction, (bottom left) terrain-perpendicular wind magnitude, and (bottom right) terrain-parallel wind magnitude at Scottsboro (K4A6) and Albertville (K8A0) for 6-h time periods leading up to first tornado in cases listed in Table 1 from 18 Mar 2013 and later.

Markowski et al. 2002). As expected, the first cloud layer tended to be higher (AGL) over the Tennessee Valley than over the Sand Mountain plateau during the 6-h period prior to tornado events in the SCS (Fig. 8). A concentration of NBL (black) points where the cloud base was lower over the Tennessee Valley is due to persistent convective precipitation ahead of the 3 October 2014 tornado event that was located over Scottsboro but did not impact Albertville. Most points tend to be within 50–150 m of each other, or approximately the difference in elevation between Scottsboro and Albertville. (Because the SCS and Tennessee Valley feature a gentle along-terrain slope upward from southwest to northeast, the mismatch in location along terrain between Albertville and Scottsboro leads to the total elevation difference being less than that of the actual valley–plateau elevation difference along a trajectory normal to the SCS and valley.) While the observed differences between first cloud layers at Scottsboro and Albertville would not suggest the likelihood of meaningful LCL height changes by themselves, the observation that the first cloud layer changes closely mimic the land elevation difference between the two sites is of particular interest. While the elevation change between Albertville and Scottsboro is only about 50 m, the gently rising slope of the SCS from southwest to northeast along its major axis means that the relief of the plateaus becomes greater to the northeast. For example, the actual relief of Sand Mountain over the Tennessee Valley where the edge of Sand Mountain makes its closest approach to Scottsboro is approximately 200 m, much larger than the 50-m difference between Albertville and Scottsboro. These observations of consistently differing first cloud layer heights, questions about whether or not these LCL changes vary in a corresponding fashion as the relief of the SCS over the surrounding terrain changes, and uncertainties surrounding how LCL variations across and around the SCS affect storm evolution are the primary motivation for the thermodynamic aspect of this study.

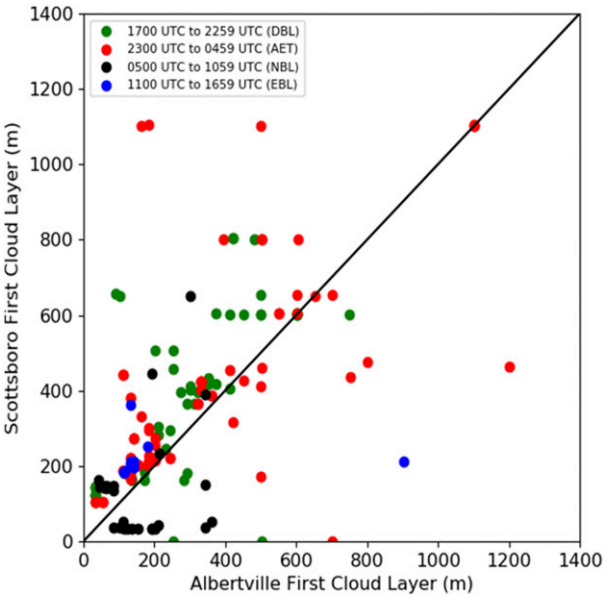

FIG. 8. As in Fig. 7, but for first cloud level.

6. RUC/RAP analysis of Froude number in SCS cases

According to Vosper et al. (2002; hereafter V02), two Froude numbers must be considered in tandem to address flow behavior over quasi-two-dimensional terrain. These Froude numbers are defined as[3] $\mathrm{Fr}_H = (U)/(NH)$ and $\mathrm{Fr}_L = (U\pi)/(NL)$, where U is the terrain-perpendicular wind component, N is the Brunt–Väisälä frequency, H is the height of the terrain feature, and L is the width of the terrain feature. According to V02, $\mathrm{Fr}_H \geq 1$ indicates that gravity waves will follow linear theory, whereas nonlinear processes such as flow splitting, flow blocking, and wave breaking may dominate at $\mathrm{Fr}_H < 1$. Fr_L determines whether or not internal gravity waves form. If $\mathrm{Fr}_L \leq 1$, then a real vertical wavenumber is realized and gravity waves form, whereas $\mathrm{Fr}_L > 1$ indicates that the vertical wavenumber is imaginary and waves are evanescent in the vertical direction.

If the atmosphere is neutrally stratified, the atmosphere over the terrain feature can be divided into an inner layer and an outer layer, where the inner layer is dominated by turbulent momentum flux divergence, and the outer layer is dominated by inertial forces. Flow over a terrain feature in a neutral atmosphere reaches a maximum U perturbation in the inner region over the crest of the terrain feature (V02). In the situation where the atmosphere is weakly stable but linear theory is valid ($\mathrm{Fr}_H \gg 1$), two possible outcomes exist. If $\mathrm{Fr}_L > 1$, then flows act very similarly to the neutral stratification cases, where a maximum in inner region flow is reached at the crest of the terrain feature. If $\mathrm{Fr}_L \leq 1$, however, gravity waves can form in the outer region, leading to pressure perturbations that can increase surface (inner layer) winds downwind of the crest of the terrain features. As Fr_L continues to decrease, the downwind acceleration of flow can increase until it surpasses the peak in flow at the

[3] V02 exclude π from the Fr_L equation. We include it here, as it is included in Stull (1988), because the factor of π indicates the relationship between an obstacle and a wavelength of the oscillation induced by the obstacle.

crest and develops into a downslope windstorm or wind enhancement.

To assess the possible role of the Froude numbers in severe storm environments over the SCS, a database of RUC/RAP upwind soundings was collected at the nearest-available 0-h forecast time prior to SCS tornado events dating back to 2006, as described in section 3. Because of the narrow, shallow nature of the Wills Valley, the entire SCS was treated as one unit in the analysis, instead of different analyses for Sand Mountain and Lookout Mountain. Heights of 150, 250, and 350 m were used as estimates for typical relief of the SCS over the surrounding terrain, and 40 km was used as a typical width scale of the SCS. Unsurprisingly, Fr_H had a magnitude much greater than 1 prior to most SCS tornado cases, owing to the relatively small relief of SCS, compared to the surrounding region, and to low values of N due to the typically weak static stability of the boundary layer in SCS tornado environments. Unlike Fr_H, Fr_L was less than 1 in both the boundary layer and free atmosphere in all cases, with the large width of the SCS dominating the calculations instead of the low values of N (Fig. 9).

Because of the dimensions of the SCS (approximately 125 km long and 40 km wide) and the oblique geometry to the mean boundary layer flow in severe storms environments, it is not immediately clear that evaluating only the component of the flow perpendicular to the primary axis of the plateaus captures the full extent of the impacts that the plateaus may have on low-level flow changes in northeast Alabama during tornado events. With this in mind, however, the end result of this cursory analysis is that given the upwind environments supplied by the RUC and the RAP, low-level acceleration of flow would be expected in the direction normal to the SCS (from approximately 140°), with a maximum likely to be reached along the northwestern slope of Sand Mountain due to the small Fr_L values. Furthermore, the large area and flat tops of the SCS plateaus suggest the potential for internal boundary layer (IBL) development (e.g., Stull 1988) due to surface friction, which could potentially further enhance low-level wind shear. Field crews deployed to the northwestern edge of Sand Mountain have reported consistently stronger winds than at other locations across the plateau or in the Tennessee Valley, bolstering the hypothesis of the existence of a low-level wind maximum in this region. One such example from a tornado outbreak on 19 March 2018, which featured an EF2 tornado on Sand Mountain, shows that surface winds observed by the UAH-SWIRLL M3V were nearly double in magnitude near the northwestern edge of the Sand Mountain plateau than over the heart of the plateau (Fig. 10). The hypothesized effect of the plateaus on the boundary layer flow, given a southerly boundary layer flow common to regional tornado-producing environments, is to cause an acceleration in the terrain-perpendicular direction that reaches a maximum on the downwind slope of the SCS, or the northwestern slope of Sand Mountain. This hypothesis will be a substantial focus of future analyses of VORTEX-SE and of numerical simulations due to the potential impacts of flow acceleration on low-level convergence, vorticity generation, and enhanced SRH in the region where tornadogenesis appears to be favored along the northwestern side of Sand Mountain.

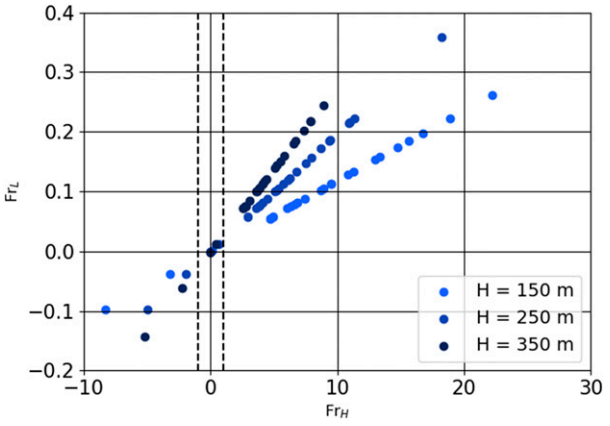

FIG. 9. RUC and RAP sounding scatterplot of Fr_H vs Fr_L at Anniston, Alabama (187 m ASL), for the most recent available 0-h model forecast times prior to SCS tornado events from 2006 to 2016. The 150-, 250-, and 350-m heights are used to display potential variations in Froude values along the SCS. The dashed lines indicated Fr_H values of −1 and 1. Note that all Fr_L values are of magnitude <1.

7. Example cases of rapid storm organization/intensification upon reaching the SCS

a. 27 April 2011: Pisgah, Alabama, EF4 supercell tornado

A pair of violent tornadoes occurred atop Sand Mountain during the 27 April 2011 tornado outbreak. The first violent tornado, rated EF4, traveled 75 km, reached a peak width of approximately 1600 m, and was responsible for 14 fatalities (Fig. 11; NCEI 2018). As shown in Fig. 11, the tornado formed along the Tennessee River in northeastern Alabama, ascended Sand Mountain near the town of Pisgah, and crossed Sand Mountain to the Wills Valley in northwestern Georgia. The tornado descended the Wills Valley, impacting the town of Trenton, Georgia, before crossing Lookout Mountain and dissipating south of Chattanooga, Tennessee.

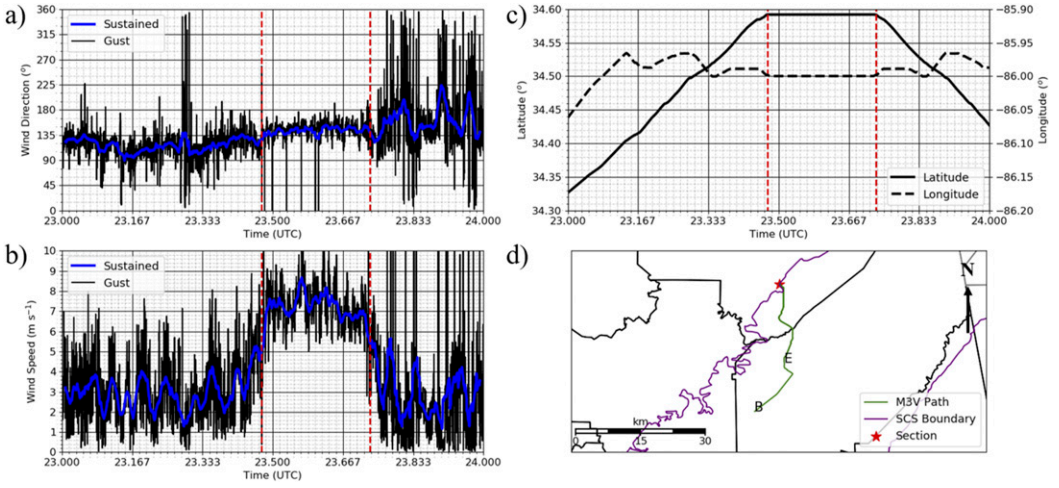

FIG. 10. (a) Wind direction and (b) wind speed measured by the UAH-SWIRLL M3V during the 2300 UTC hour on 19 Mar 2018, exemplifying the systematic increase in surface winds noted by field crews at the northwestern edge of the Sand Mountain plateau. (c) Latitude and longitude of M3V during the hour and (d) the path taken by M3V atop the SCS. The red dashed lines in (a)–(c) indicate the time period that M3V was stopped at Section, Alabama, at the red star in (d). The "B" and "E" markers in (d) indicate the start and end points of M3V during the hour, respectively, with M3V traveling from point B to Section, stopping at Section, and then traveling over the same path back to point E.

A single-Doppler analysis was performed on data from the WSR-88D radar at Hytop, Alabama (KHTX), to characterize the changes in size and intensity of the detected circulation associated with the Pisgah tornadic supercell. The parent supercell mesocyclone moved from the Tennessee River valley to atop Sand Mountain at around 2100 UTC (Fig. 12). Rapid intensification of the parent mesocyclone and the tornado cyclone occurred as the circulation moved atop Sand Mountain, with EF1 damage noted on the northwest slopes of Sand Mountain and intensification to EF3 to EF4 strength upon reaching the top of Sand Mountain (Fig. 5). Analysis of V_{ROT} of the detected circulation confirms the rapid intensification, with a rapid increase of V_{ROT} from 24.7 to 50.6 m s^{-1} noted at the 0.5° elevation angle (the lowest elevation angle) between 2102 and 2111 UTC (Fig. 13). Similar rapid intensification of low-level mesocyclones and subsequent tornadogenesis as supercells move atop Sand Mountain has been seen in additional past cases. Investigation of these rapid low-level mesocyclone intensification episodes and their potential physical causes, either by influence from near-storm

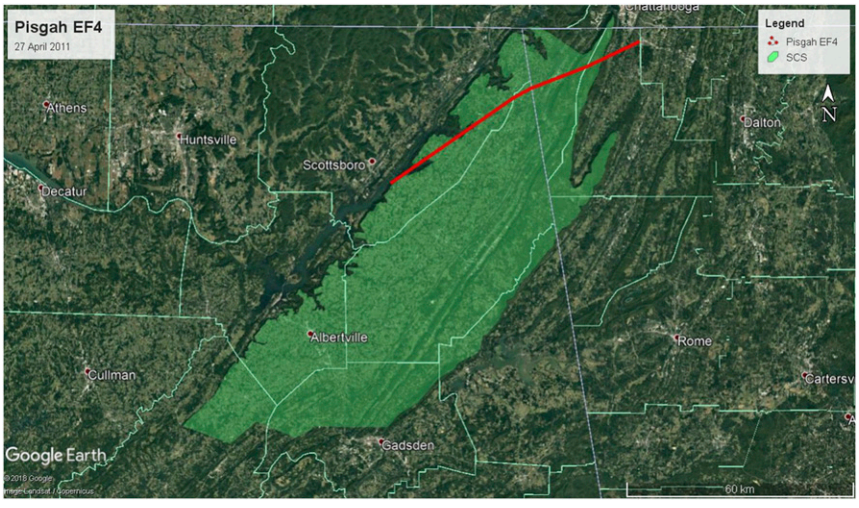

FIG. 11. Overview map of the Pisgah EF4 tornado track from 27 Apr 2011.

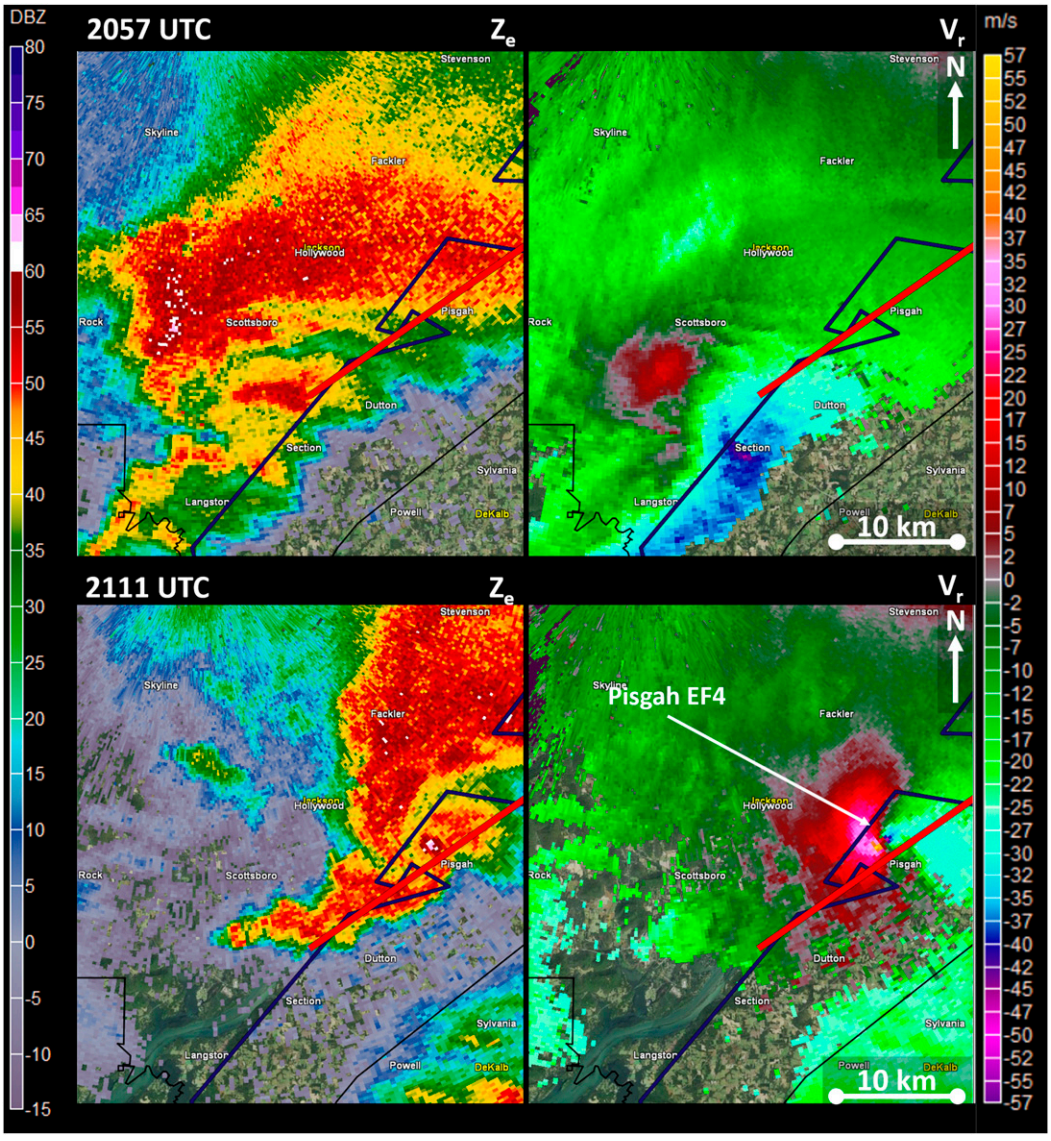

FIG. 12. (left) Equivalent reflectivity factor (Z_e) and (right) radial velocity (V_r) PPIs from the Hytop, Alabama (KHTX), WSR-88D at 2057 and 2116 UTC 27 Apr 2011.The couplet center ranged from 32.4 to 34.4 km away from KHTX. The navy line indicates the northwestern edge of the SCS.

environmental changes or by processes internal to the storm, will be a focus for further study, including analysis of datasets collected during VORTEX-SE.

b. 25 October 2010: Section, Henagar-Ider, and Pisgah-Rosalie, Alabama, QLCS tornadoes

A severe QLCS event transpired across northern Alabama during the predawn hours of 25 October 2010. After producing an EF1 tornado and numerous nontornadic wind damage reports across northwestern and north-central Alabama, the QLCS produced four tornadoes across northeastern Alabama. Three of these four tornadoes occurred within the SCS: one of EF0 damage intensity, one of EF1 damage intensity, and one of EF2 damage intensity (Fig. 14). The EF0 and EF2 tornadoes were produced by the same parent mesovortex, which formed along the northwestern slope of Sand Mountain near Section and continued northeastward into Georgia. The EF0 was a brief tornado at Section, with a pathlength of 3.5 km, and the EF2 began near the town of Rosalie and moved east-northeast for 32.6 km, through the towns of Henagar and Ider and across the state line into Georgia. The EF1 formed within a mesovortex that quickly intensified along the northwestern edge of Sand Mountain near Pisgah, just north of the Section mesovortex. The tornado

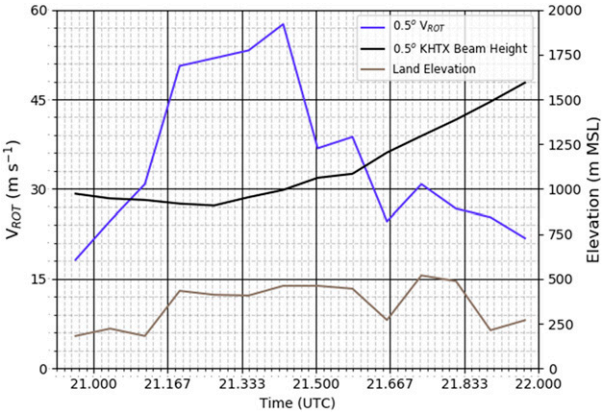

FIG. 13. Time series plots of rotational velocity (V_{ROT}), 0.5° beam height, and land elevation for the 27 Apr 2011 Pisgah, Alabama, EF4 tornado.

traveled 25.2 km, moving through the southern end of Rosalie before crossing the Jackson/DeKalb County line near Ider before it dissipated and the parent mesovortex merged with the Section–Henagar-Ider mesovortex (Fig. 15).

The 25 October 2010 case represents a behavior often seen in QLCSs as they reach the northwestern edge of Sand Mountain. Often, the shear zone along the gust front will appear to strengthen, occasionally leading to the development of mesovortices. It is unclear whether this development or intensification of mesovortices is due to increased low-level wind shear, an increase in horizontal shear and associated horizontal shear instability as the gust front moves atop the plateau, or an increase in low-level convergence and stretching of vertical vorticity, all of which have been linked to potential mesovortex genesis or intensification (Atkins and St. Laurent 2009; Wheatley and Trapp 2008). The propensity for mesovortex genesis in QLCSs that move atop Sand Mountain and the potential causes for this behavior are a planned focus of future intensive study.

8. Analysis and discussion

Preliminary observations and analyses from tornado events in the SCS indicate several potential physical processes that may lead to enhanced tornado potential versus surrounding areas, given at least a marginally favorable background environment for tornadoes. The wind tendency indicates at least the potential for forced channeling of flow [as defined by Whiteman and Doran (1993)] up the valley (toward the northeast), given that the flow is generally kept in the same general direction as the upstream flow. The diurnal variability contradicts what would be expected for a thermally driven channeling, in which the greater down-valley flow (toward the southwest) would be expected at night, whereas more up-valley flow is observed during nocturnal hours in these cases. Pressure-driven channeling also does not appear to be supported since there is no hard evidence of a countercurrent to the ambient geostrophic flow. Additionally, the acceleration of the flow atop Sand Mountain in the terrain-perpendicular direction appears to corroborate what would theoretically be expected, based on the RUC/RAP sounding analyses in section 6. The predominance of $\mathrm{Fr}_H \gg 1$ and $\mathrm{Fr}_L \leq 1$ values across the soundings (Fig. 9) indicate that the terrain-perpendicular component of the flow across the SCS should generally accelerate within the boundary layer, with a maximum near the "crest" of the terrain and a second maximum in flow on the downslope (i.e., a

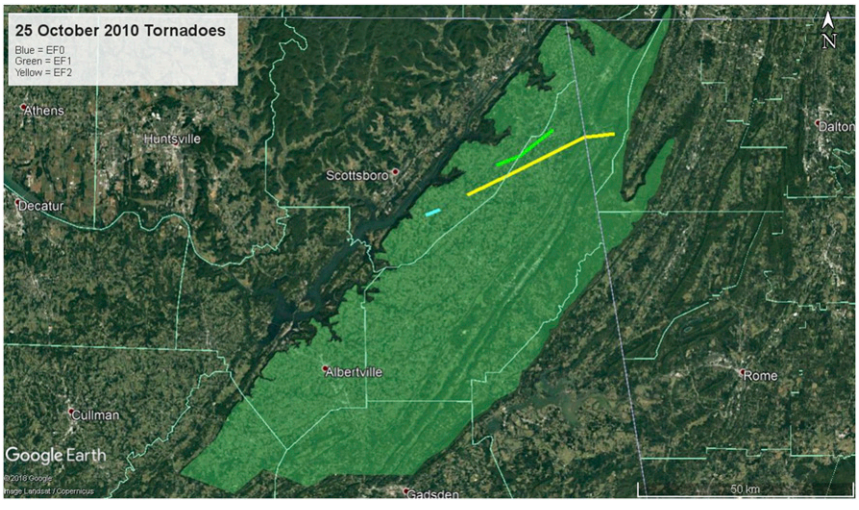

FIG. 14. Overview map of the 25 Oct 2010 tornado tracks across the SCS.

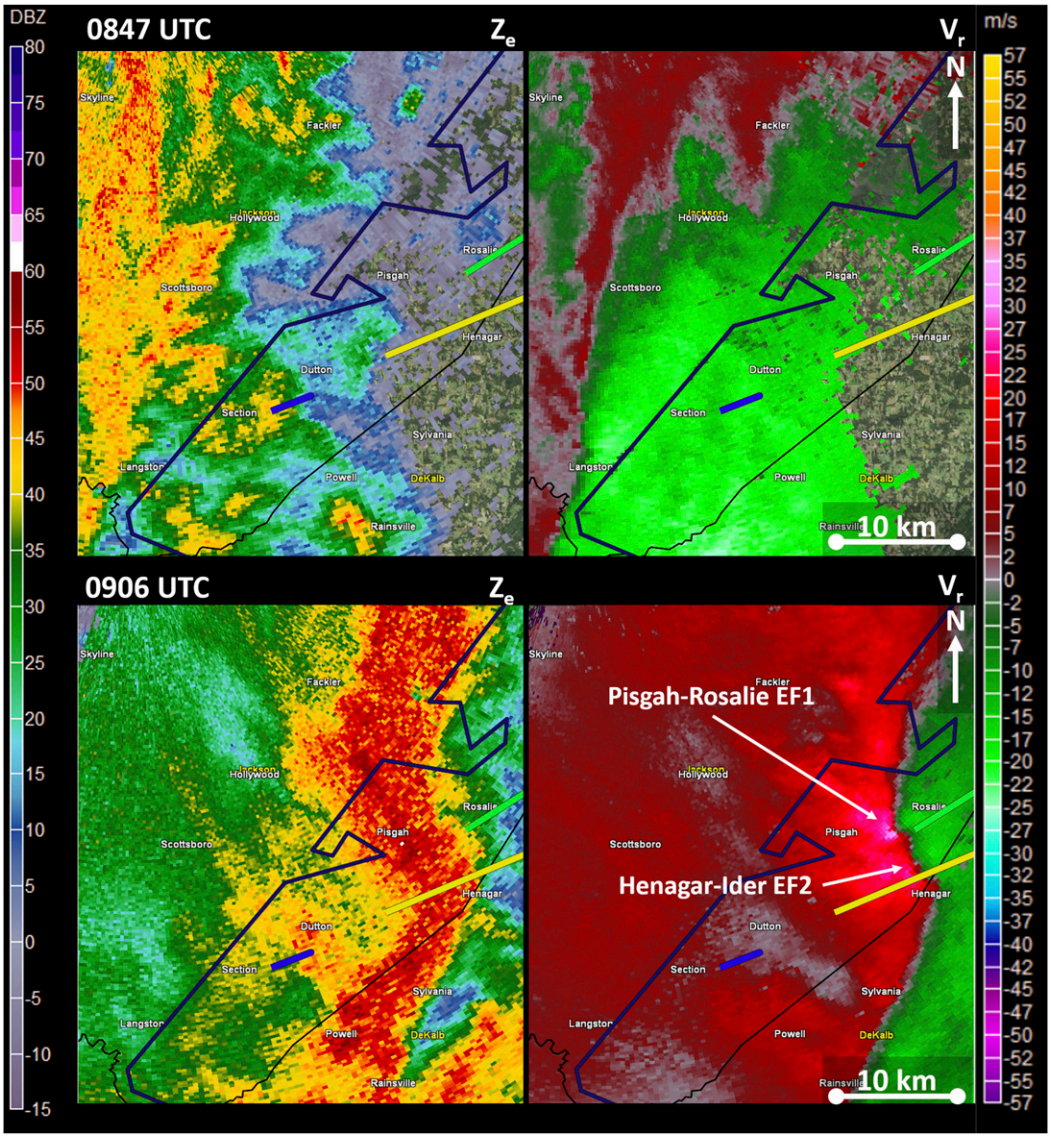

FIG. 15. (left) Equivalent reflectivity factor (Z_e) and (right) radial velocity (V_r) PPIs from the Hytop, Alabama (KHTX), WSR-88D at 0847 and 0906 UTC 25 Oct 2010.

downslope flow enhancement or windstorm). Although observations currently available to support the downslope enhancement are limited to a small handful of point surface observations by field crews on a limited number of deployments and are largely qualitative in nature, the tendency for backed and stronger surface flow atop the plateau at Albertville versus in the valley at Scottsboro supports the potential for this acceleration pattern to exist and prompts further observations and analysis, particularly through numerical simulations. These observations were used as the motivation for beginning detailed wind-profiling observations around the SCS during severe weather events to investigate how persistent and how deep the flow modifications are and how they may impact SRH, vertical vorticity, and convergence across the SCS. Findings from these observational deployments will be detailed in later articles.

Similar to the analyses of terrain-perpendicular and terrain-parallel flow, a comparative analysis was performed for first cloud layers from the ceilometers at K8A0 and K4A6. As discussed in section 3, these data are used as proxies for LCL height, which has been found to be a meaningful discriminator in significant tornado versus nontornadic environments. As expected, the first cloud layer tended to be higher over the Tennessee Valley (326-m mean; 259-m standard deviation) than over the Sand Mountain plateau (282-m mean; 245-m standard deviation) leading up to tornado events

in the SCS (Fig. 8). A concentration of NBL (black) points where the cloud base was lower over the Tennessee Valley is due to persistent convective precipitation ahead of the 3 October 2014 tornado event that was located over Scottsboro but did not impact Albertville. Most points tend to be within 50–150 m of each other, or approximately the difference in elevation between Scottsboro and Albertville. These observations of consistently differing first cloud layer heights are the primary motivation for the thermodynamic aspect of this study, particularly on how LCL height varies around the SCS and what effects that variation may have on the propensity for tornadogenesis in the region.

The dimensions, orientation, and complexities of the SCS terrain introduce significant uncertainty as to how wind profiles in particular may realistically evolve in a severe storm environment. Although the Froude numbers indicate that low-level flow should accelerate in the terrain-perpendicular direction, the large, relatively flat tops of the Sand Mountain and Lookout Mountain plateaus suggest the potential for a substantial mechanically induced IBL to develop within the flow. It is unclear whether or not IBL development negates the acceleration of the flow induced by the plateaus or simply acts to further increase low-level wind shear by reducing the wind speed near the surface while the flow aloft within the ''inner layer'' of flow is still accelerated over the plateaus. Additionally, the south-southwest to north-northeast orientations of Sand Mountain and Lookout Mountain lead to a substantial component of ambient boundary layer flow that is parallel to the axes of the plateaus and the adjacent Tennessee and Wills Valleys. Furthermore, as previously discussed in section 5, the reliefs of both Sand Mountain and Lookout Mountain from the surrounding lower lands generally increase slowly from south-southwest to north-northeast. It is not immediately clear that the terrain-perpendicular direction is the most relevant direction over which flow may be accelerated, nor is it obvious how the along-axes (terrain parallel) flow may evolve in a severe storm environment. These questions will also be examined in the context of VORTEX-SE and other observational and numerical simulation datasets.

The primary consequence of the longer-term datasets described in this article is that there may be numerous potential physical causes for the apparent maximum in tornado activity in the SCS region. Changes in flow due to acceleration over the plateaus may lead to SRH changes, development of convergence, and development of vorticity. The upstream Froude numbers imply that acceleration may be maximized near the northwestern edge of Sand Mountain, which implies that the above effects may also be maximized in this region. Additionally, storms moving from the Tennessee Valley to the Sand Mountain plateau would first reach the area of potentially lower LCL heights along the northwestern side of Sand Mountain. Though it is unclear how long it would take for a particular storm to experience changes in the rate of evaporational cooling in the RFD and subsequent RFD buoyancy, all of the above factors may lead to physical explanations for why the SCS not only appears to be a maximum in tornado activity, but more specifically why the northwestern edge of the Sand Mountain plateau appears to be a region of particular proclivity for tornadogenesis and why the development and/or intensification of rotation in storms crossing the northwestern edge of the plateau can occur very quickly, as detailed in the cases shown in section 7. The main overarching question may be whether or not environmental parcels ingested into storms along the northwest side of Sand Mountain are able to attain enhancement in (vertical) vorticity similar to that within more conventional atmospheric baroclinic boundaries (e.g., Markowski et al. 1998; Rasmussen et al. 2000; Wheatley and Trapp 2008). However, no evidence has yet been found to this point to suggest that topographic enhancements in vorticity may rival those seen along baroclinic boundaries.

9. Conclusions

An apparent maximum in tornado activity appears to exist across the northeastern portion of Alabama, across the Sand Mountain and Lookout Mountain plateaus, which were defined herein as the Southern Cumberland System (SCS). This region displays a higher rate of historical tornado activity when compared to surrounding areas, particularly to the north and south of the plateaus. Furthermore, a close examination of tornado activity across the SCS reveals a distinct tendency for tornadogenesis to occur in close proximity to the northwestern edge of the Sand Mountain plateau. Longtime operational meteorologists serving northeastern Alabama have anecdotally noted that storm intensification and tornado development in the SCS tends to occur rapidly. These observations are supported by the generally poor probability of detection and lead time statistics for tornadogenesis across the region, which are not only limited to weak tornadoes or tornadoes formed by QLCSs, but also extended to supercellular and strong tornadoes. The cases detailed in section 7 showcase how this observed rapid evolution and intensification upon crossing atop Sand Mountain can occur in both supercells and QLCSs.

Although long-term meteorological observations are rather scant across northeastern Alabama, information

can be gleaned from a few surface stations, as well as from past RUC/RAP model guidance. RUC/RAP guidance from past SCS tornado events suggests that low-level acceleration in flow in the terrain-perpendicular direction should occur given upstream values of the Froude number, with acceleration occurring over the crests of the plateaus and at least the potential for further acceleration within the downslope regions of the plateaus. Though the downslope accelerations cannot be observed in the long-term datasets, long-term surface data comparisons from Albertville (atop Sand Mountain) and Scottsboro (in the Tennessee Valley) ahead of SCS tornado events show that such acceleration may indeed occur, with surface flow tending to be stronger and more backed atop the plateau than in the valley. It is unclear from these observations how high above ground this acceleration extends or how the wind shear profile is affected.

The exploratory research detailed in this manuscript was used to inform experiments ahead of and during the VORTEX-SE 2017 field campaign. Numerous datasets were gathered for tornadic and potentially tornadic severe weather events in northeastern Alabama from November 2016 through June 2017. The primary method of observational analysis was through the deployment of numerous profiling systems and sounding teams around the SCS and surrounding region to gather comparative datasets of vertical kinematic and thermodynamic profiles in different regions of the terrain system. Analysis of these datasets is ongoing. Additionally, numerical simulation studies have been undertaken for events in northeastern Alabama to further inform how the near-storm environment may be impacted by the SCS and surrounding topographic features. These robust datasets and simulation studies will be used to either further develop or refute ideas posed in this paper and to develop more sophisticated hypotheses for the overall role of the SCS in severe storm and tornado evolution in northeastern Alabama. The end goal of this research will be to develop conceptual models of how the SCS may impact severe storm evolution and tornado potential, which can then be transitioned into helpful guidance for the operational community.

Acknowledgments. The authors thank Dr. P. Grady Dixon (Fort Hays State University) for assistance in the optimized hot spot analysis of tornadogenesis presented in this paper. This work was completed as parts of a Master of Science thesis and Doctor of Philosophy dissertation by the lead author. Funding for this research was provided by the University of Alabama in Huntsville's Earth System Science Center (UAH ESSC), NSF Grant AGS-1359771, NOAA Grant NA16OAR4590216, and NOAA subcontract 191001.363513.04D from the Northern Gulf Institute (through Mississippi State University).

REFERENCES

ArcGIS, 2018: How optimized hot spot analysis works. ArcGIS Pro, http://pro.arcgis.com/en/pro-app/tool-reference/spatial-statistics/how-optimized-hot-spot-analysis-works.htm.

Ashley, W. S., 2007: Spatial and temporal analysis of tornado fatalities in the United States: 1880–2005. *Wea. Forecasting*, **22**, 1214–1228, https://doi.org/10.1175/2007WAF2007004.1.

——, A. J. Krmenec, and R. Schwantes, 2008: Vulnerability due to nocturnal tornadoes. *Wea. Forecasting*, **23**, 795–807, https://doi.org/10.1175/2008WAF2222132.1.

Atkins, N. T., and M. St. Laurent, 2009: Bow echo mesovortices. Part II: Their genesis. *Mon. Wea. Rev.*, **137**, 1514–1532, https://doi.org/10.1175/2008MWR2650.1.

Bluestein, H. B., 2000: A tornadic supercell over elevated, complex terrain: The Divide, Colorado, storm of 12 July 1996. *Mon. Wea. Rev.*, **128**, 795–809, https://doi.org/10.1175/1520-0493(2000)128<0795:ATSOEC>2.0.CO;2.

——, J. B. Houser, M. M. French, J. C. Snyder, G. D. Emmitt, I. PopStefanija, C. Baldi, and R. T. Bluth, 2014: Observations of the boundary layer near tornadoes and in supercells using a mobile, collocated, pulsed Doppler lidar and radar. *J. Atmos. Oceanic Technol.*, **31**, 302–325, https://doi.org/10.1175/JTECH-D-13-00112.1.

Bosart, L. F., A. Seimon, K. D. LaPenta, and M. J. Dickinson, 2006: Supercell tornadogenesis over complex terrain: The Great Barrington, Massachusetts, tornado on 29 May 1995. *Wea. Forecasting*, **21**, 897–922, https://doi.org/10.1175/WAF957.1.

Braun, S. A., and J. P. Monteverdi, 1991: An analysis of a mesocyclone–induced tornado occurrence in Northern California. *Wea. Forecasting*, **6**, 13–31, https://doi.org/10.1175/1520-0434(1991)006<0013:AAOAMT>2.0.CO;2.

Bryan, G. H., and J. M. Fritsch, 2002: A benchmark simulation for moist nonhydrostatic numerical models. *Mon. Wea. Rev.*, **130**, 2917–2928, https://doi.org/10.1175/1520-0493(2002)130<2917:ABSFMN>2.0.CO;2.

Coleman, T. A., and P. G. Dixon, 2014: An objective analysis of tornado risk in the United States. *Wea. Forecasting*, **29**, 366–376, https://doi.org/10.1175/WAF-D-13-00057.1.

Desrochers, P. R., and F. I. Harris, 1996: Interpretation of mesocyclone vorticity and divergence structure from single-Doppler radar. *J. Appl. Meteor.*, **35**, 2191–2209, https://doi.org/10.1175/1520-0450(1996)035<2191:IOMVAD>2.0.CO;2.

Dixon, P. G., A. E. Mercer, J. Choi, and J. S. Allen, 2011: Tornado risk analysis: Is Dixie Alley an extension of Tornado Alley? *Bull. Amer. Meteor. Soc.*, **92**, 433–441, https://doi.org/10.1175/2010BAMS3102.1.

Doswell, C. A., III, 2014: My version of tornado myths. http://www.flame.org/~cdoswell/Tornado_Mythology.html.

Forbes, G. S., 1998: Topographic influences on tornadoes in Pennsylvania. Preprints, *19th Conf. on Severe Local Storms*, Minneapolis, MN, Amer. Meteor. Soc., 269–272.

Fujita, T. T., 1989: The Teton-Yellowstone tornado of 21 July 1987. *Mon. Wea. Rev.*, **117**, 1913–1940, https://doi.org/10.1175/1520-0493(1989)117<1913:TTYTOJ>2.0.CO;2.

Gaffin, D. M., and S. S. Parker, 2006: A climatology of synoptic conditions associated with significant tornadoes across the southern Appalachian region. *Wea. Forecasting*, **21**, 735–751, https://doi.org/10.1175/WAF951.1.

Geerts, B., T. Andretta, S. Luberda, J. Vogt, Y. Wang, L. D. Oolman, J. Finch, and D. Bikos, 2009: A case study of a long-lived tornadic mesocyclone in a low-CAPE complex-terrain environment. *Electron. J. Severe Storms Meteor.*, **4** (3), 1–29.

Getis, A., and J. K. Ord, 1992: The analysis of spatial association by use of distance statistics. *Geogr. Anal.*, **24**, 189–206, https://doi.org/10.1111/j.1538-4632.1992.tb00261.x.

Goodman, S. J., and K. R. Knupp, 1993: Tornadogenesis via squall line and supercell interaction: The November 15, 1989, Huntsville, Alabama, tornado. *The Tornado: Its Structure, Dynamics, Prediction, and Hazards*, *Geophys. Monogr.*, Vol. 79, Amer. Geophys. Union, 183–199.

Houser, J. B., K. M. Butler, and N. McGinnis, 2017: Correlations between topography and land cover with tornado intensity using rapid-scan mobile and WSR-88D radar observations in a geographic information system framework. *38th Conf. on Radar Meteorology*, Chicago, IL, Amer. Meteor. Soc., KS10.1, https://ams.confex.com/ams/38RADAR/webprogram/Paper320671.html.

Karstens, C. D., W. A. Gallus Jr., B. D. Lee, and C. A. Finley, 2013: Analysis of tornado-induced tree fall using aerial photography from the Joplin, Missouri, and Tuscaloosa–Birmingham, Alabama, tornadoes of 2011. *J. Appl. Meteor. Climatol.*, **52**, 1049–1068, https://doi.org/10.1175/JAMC-D-12-0206.1.

Kis, A. K., and J. M. Straka, 2010: Nocturnal tornado climatology. *Wea. Forecasting*, **25**, 545–561, https://doi.org/10.1175/2009WAF2222294.1.

Knupp, K. R., and Coauthors, 2014: Meteorological overview of the devastating 27 April 2011 tornado outbreak. *Bull. Amer. Meteor. Soc.*, **95**, 1041–1062, https://doi.org/10.1175/BAMS-D-11-00229.1.

Krocak, M. J., and H. E. Brooks, 2018: Climatological estimates of hourly tornado probability for the United States. *Wea. Forecasting*, **33**, 59–69, https://doi.org/10.1175/WAF-D-17-0123.1.

LaPenta, K. D., L. F. Bosart, T. J. Galarneau, and M. J. Dickinson, 2005: A multiscale examination of the 31 May 1998 Mechanicville, New York, tornado. *Wea. Forecasting*, **20**, 494–516, https://doi.org/10.1175/WAF875.1.

Lewellen, D. W., 2012: Effects of topography on tornado dynamics: A simulation study. *26th Conf. on Severe Local Storms*, Nashville, TN, Amer. Meteor. Soc., 4B.1, https://ams.confex.com/ams/26SLS/webprogram/Paper211460.html.

——, and W. S. Lewellen, 2007: Near-surface vortex intensification through corner flow collapse. *J. Atmos. Sci.*, **64**, 2195–2209, https://doi.org/10.1175/JAS3966.1.

Markowski, P. M., and N. Dotzek, 2011: A numerical study of the effects of orography on supercells. *Atmos. Res.*, **100**, 457–478, https://doi.org/10.1016/j.atmosres.2010.12.027.

——, E. N. Rasmussen, and J. M. Straka, 1998: The occurrence of tornadoes in supercells interacting with boundaries during VORTEX-95. *Wea. Forecasting*, **13**, 852–859, https://doi.org/10.1175/1520-0434(1998)013<0852:TOOTIS>2.0.CO;2.

——, J. M. Straka, and E. N. Rasmussen, 2002: Direct surface thermodynamic observations within the rear-flank downdrafts of nontornadic and tornadic supercells. *Mon. Wea. Rev.*, **130**, 1692–1721, https://doi.org/10.1175/1520-0493(2002)130<1692:DSTOWT>2.0.CO;2.

Marshall, T. P., J. R. McDonald, and G. S. Forbes, 2004: The Enhanced Fujita (EF) scale. *22nd Conf. on Severe Local Storms*, Hyannis, MA, Amer. Meteor. Soc., 3B.2, https://ams.confex.com/ams/11aram22sls/techprogram/paper_81090.htm.

McDonald, L., 2014: Tornadoes in the Boston Mountains of northern Arkansas. TheWeatherPrediction.com, http://theweatherprediction.com/weatherpapers/103/index.html.

MoDOT, 2018: Automated weather observing system. Missouri Department of Transportation, https://www.modot.org/automated-weather-observing-system.

Monteverdi, J. P., R. Edwards, and G. J. Stumpf, 2014: An analysis of the 7 July 2004 Rockwell Pass, California, tornado: Highest-elevation tornado documented in the United States. *Mon. Wea. Rev.*, **142**, 3925–3943, https://doi.org/10.1175/MWR-D-14-00222.1.

NCEI, 2018: *Storm Data.* NOAA/NCEI, https://www.ncdc.noaa.gov/IPS/sd/sd.html.

Nuss, W. A., 1986: Observations of a mountain tornado. *Mon. Wea. Rev.*, **114**, 233–237, https://doi.org/10.1175/1520-0493(1986)114<0233:OOAMT>2.0.CO;2.

Petersen, W. A., and Coauthors, 2005: The UAH-NSSTC/WHNT ARMOR C-band dual-polarimetric radar: A unique collaboration in research, education, and technology transfer. *32nd Conf. on Radar Meteorology*, Albuquerque, NM, Amer. Meteor. Soc., 12R.4, https://ams.confex.com/ams/32Rad11Meso/techprogram/paper_96524.htm.

Rankine, W. J. M., 1901: *A Manual of Applied Mechanics*. 16th ed. Charles Griffin and Company, 680 pp.

Rasmussen, E. N., and D. O. Blanchard, 1998: A baseline climatology of sounding-derived supercell and tornado forecast parameters. *Wea. Forecasting*, **13**, 1148–1164, https://doi.org/10.1175/1520-0434(1998)013<1148:ABCOSD>2.0.CO;2.

——, S. Richardson, J. M. Straka, P. M. Markowski, and D. O. Blanchard, 2000: The association of significant tornadoes with a baroclinic boundary on 2 June 1995. *Mon. Wea. Rev.*, **128**, 174–191, https://doi.org/10.1175/1520-0493(2000)128<0174:TAOSTW>2.0.CO;2.

Schneider, D. G., 2009: The impact of terrain on three cases of tornadogenesis in the Great Tennessee Valley. *Electron. J. Operational Meteor.*, **10** (11), 1–33.

Shamburger, S. W., 2012: Higher terrain impacts of eastern middle Tennessee on tornadogenesis. *26th Conf. on Severe Local Storms*, Nashville, TN, Amer. Meteor. Soc., 9, https://ams.confex.com/ams/26SLS/webprogram/Paper211577.html.

Stull, R. B., 1988: *An Introduction to Boundary Layer Meteorology*. Springer, 670 pp.

Ventura, V., C. J. Paciorek, and J. S. Risbey, 2004: Controlling the proportion of falsely rejected hypotheses when conducting multiple tests with climatological data. *J. Climate*, **17**, 4343–4356, https://doi.org/10.1175/3199.1.

Vosper, S. B., S. D. Mobbs, and B. A. Gardiner, 2002: Measurements of the near-surface flow over a hill. *Quart. J. Roy. Meteor. Soc.*, **128**, 2257–2280, https://doi.org/10.1256/qj.01.11.

Wheatley, D. M., and R. J. Trapp, 2008: The effect of mesoscale heterogeneity on the genesis and structure of mesovortices within quasi-linear convective systems. *Mon. Wea. Rev.*, **136**, 4220–4241, https://doi.org/10.1175/2008MWR2294.1.

Whiteman, C. D., and J. C. Doran, 1993: The relationship between overlying synoptic-scale flows and winds within a valley. *J. Appl. Meteor.*, **32**, 1669–1682, https://doi.org/10.1175/1520-0450(1993)032<1669:TRBOSS>2.0.CO;2.